Received: 6 February 2021 | Revised: 15 April 2021 | Accepted: 26 April 2021

DOI: 10.1002/hbm.25539

RESEARCH ARTICLE

WILEY

The balance between Bayesian inference and default mode determines the generation of tinnitus from decreased auditory input: A volume entropy-based study

Jae-Jin Song[1] | Jaemin Park[2] | Ja-Won Koo[1] | Sang-Yeon Lee[1] | Sven Vanneste[3] | Dirk De Ridder[4] | Soonki Hong[2] | Seonhee Lim[2]

[1]Department of Otorhinolaryngology-Head and Neck Surgery, Seoul National University Bundang Hospital, Seongnam, South Korea

[2]Department of Mathematical Sciences, Seoul National University, Seoul, South Korea

[3]Lab for Clinical & Integrative Neuroscience, Trinity College of Neuroscience, Trinity College Dublin, Ireland

[4]Unit of Neurosurgery, Department of Surgical Sciences, Dunedin School of Medicine, University of Otago, Dunedin, New Zealand

Correspondence
Jae-Jin Song, Department of Otorhinolaryngology-Head and Neck Surgery, Seoul National University Bundang Hospital, 166 Gumi-Ro, Bundang-Gu, Gyeonggi-Do, 463-707, South Korea.
Email: jjsong96@snubh.org; jjsong96@gmail.com

Seonhee Lim, Department of Mathematical Science and Research Institute of Mathematical Sciences, Seoul National University, 1 Gwanak-ro, Gwanak-gu, Seoul, 151-742, South Korea.
Email: slim@snu.ac.kr

Funding information
BK21 PLUS SNU Mathematical Sciences Division; Industrial and Mathematical Data Analytics Research Center, Grant/Award Number: 0679-20200002; National Research Foundation of Korea, Grant/Award Numbers: 2017R1E1A1A03070779, 2019R1A2C2004941; Seoul National University Bundang Hospital, Grant/Award Number: 14-2019-033

Abstract

Along with phantom pain, tinnitus, a phantom auditory perception occurring in the absence of an external acoustic stimulus, is one of the most representative phantom perceptions that develops in subjects with decreased peripheral sensory input. Although tinnitus is closely associated with peripheral hearing loss (HL), it remains unclear why only some individuals with HL develop tinnitus. In this study, we investigated the differences between 65 HL with tinnitus (HL-T) and 104 HL with no tinnitus (HL-NT) using a resting-state electroencephalography data-based volume entropy model of the brain network, by comparing the afferent node capacities, that quantify the contribution of each node to the spread of information, of all Brodmann areas. While the HL-T group showed increased information flow in areas involved in Bayesian inference (the left orbitofrontal cortex, the left subgenual anterior cingulate cortex, and the left ventrolateral prefrontal cortex) and auditory memory storage (the right hippocampus/parahippocampus), the HL-NT group showed increased afferent node capacity in hub areas of the default mode network (DMN; the right posterior cingulate cortex and the right medial temporal gyrus). These results suggest that the balance of activity between the Bayesian inferential network (updating missing auditory information by retrieving auditory memories from the hippocampus/parahippocampus) and DMN (maintaining the "silent status quo") determines whether phantom auditory perception occurs in a brain with decreased peripheral auditory input.

KEYWORDS
Bayesian, deafferentation, default mode, memory, tinnitus

Jae-Jin Song and Jaemin Park contributed equally to this work.

1 | INTRODUCTION

Non-pulsatile subjective tinnitus is a phantom auditory perception occurring in the absence of an external acoustic stimulus (Lee et al., 2017). The prevalence of tinnitus has been reported to be 6–22% (Axelsson & Ringdahl, 1989; Gallus et al., 2015; Kim et al., 2015; Shargorodsky, Curhan, & Farwell, 2010; Wu, Searchfield, Exeter, & Lee, 2015) and increases with age (Oiticica & Bittar, 2015; Wu et al., 2015); tinnitus represents a social burden in aging societies.

Possible mechanisms suggested for the generation of tinnitus can be classified into three broad categories: (a) peripheral auditory deafferentation and central maladaptive plastic changes, (b) spontaneous auditory neuronal hyperactivity, and (c) increased cross-fiber synchrony among neurons (Baguley, McFerran, & Hall, 2013; Eggermont & Roberts, 2012). Previous studies have identified correlations between tinnitus pitch and the frequency of maximum hearing loss (HL) (Schaette, Turtle, & Munro, 2012; Schecklmann et al., 2012), suggesting that tinnitus may be a "fill-in phenomenon" for missing auditory information due to HL. In animal studies, subsequent pathologic changes in the central auditory system linked HL to tinnitus (Lee et al., 2017; Norena & Eggermont, 2005; Norena, Micheyl, Chery-Croze, & Collet, 2002). Recent animal and human studies have also indicated that HL should be preceded by auditory experience to generate tinnitus (Eggermont & Kral, 2016; Lee et al., 2017).

However, there are still a number of unanswered questions concerning the generation of tinnitus in subjects with HL. Although most cases of tinnitus are closely associated with HL or auditory deafferentation, not all individuals with HL develop tinnitus. This suggests that the filling in of missing auditory information does not occur in every individual with HL. Most commonly, HL originates from changes in the peripheral auditory system while tinnitus is generated in the brain. This suggests that different neural substrates may exist between hearing loss with tinnitus (HL-T) and hearing loss without the generation of tinnitus (HL-NT). Resting-state quantitative electroencephalography (rs-qEEG) may be able to identify the central mechanism that links HL to auditory phantom perception based on the fill-in phenomenon.

To determine if there were differences in resting-state cortical activity between the HL-T and HL-NT groups at the brain network level, we adopted the "volume entropy model" (Lee et al., 2019) and compared the groups with respect to information flow in the brain. The volume entropy of the brain network corresponds to the limit of asymptotic exponential growth rate of the number of paths in the network (Lee, Kim, et al., 2019). As a global measure of the brain network, volume entropy represents the global efficiency of the propagation of information throughout the brain network. Furthermore, we can obtain a local measure at each brain region based on the afferent node capacity, which is another marker of volume entropy. Afferent node capacity, which is associated with volume entropy, quantifies the contribution of each node to the spread of information.

Although the volume entropy model has not priory been adopted in tinnitus-related studies, based on precedent functional neuroimaging studies of the pathophysiology of tinnitus, our a priori hypothesis was that while the HL-T group may generate tinnitus by retrieving stored auditory memory (Vanneste & De Ridder, 2016) to fill in for the lost peripheral auditory input (De Ridder, Vanneste, & Freeman, 2014), the HL-NT group may not develop unnecessary tinnitus in spite of peripherally decreased auditory input with the help of cortical areas involved in maintaining unfocused resting-state. In this regard, we hypothesized that the HL-T group would exhibit increased afferent node capacity in the cortical areas in charge of memory and Bayesian inference, to reduce perceptual uncertainty by generating tinnitus in response to decreased peripheral auditory input (De Ridder, Joos, & Vanneste, 2014; De Ridder, Vanneste, & Freeman, 2014). Meanwhile, the HL-NT group was expected to show relatively increased afferent node capacity in areas involved in the maintenance of the task-free resting state of the brain, such as the default mode network (DMN) (Raichle et al., 2001; Raichle & Snyder, 2007), which are not affected by decreased auditory information. To test our hypotheses, we used the volume entropy model to compare the HL-T and HL-NT groups in terms of rs-qEEG data for cortical areas showing significantly different information flow, and discuss possible reasons for tinnitus generation in the HL-T group and non-generation in the HL-NT group.

2 | MATERIALS AND METHODS

2.1 | Participants

All procedures in this study were approved by the institutional review boards of Seoul National University Bundang Hospital (IRB-B-2006-621-105) and the need for informed consent from the participants has been waived by the IRB. Table 1 summarizes the characteristics of the two groups. A total of 65 tinnitus patients with bilateral HL from the database of Seoul National University Bundang Hospital were included in the HL-T group. The average hearing threshold (average of the pure tone audiometry [PTA] thresholds at 500, 1,000, 2,000, and 4,000 Hz) of the subjects in the HL-T group was more than 25 dB HL bilaterally. The mean age of the participants in the HL-T group was 66.6 ± 10.1 years (range: 32–82 years), and 21 (32.3%) were male. Of 65 subjects, 39 (60%) reported pure-tone tinnitus while the remaining 26 (40%) reported narrow-band noise tinnitus. A total of 44 (67.78%) subjects had bilateral tinnitus while the remaining 21 had unilateral tinnitus.

For the HL-NT group, 104 hearing threshold-matched individuals with bilateral HL (> 25 dB) without tinnitus were selected from our database. The mean age of the HL-NT group was 67.5 ± 13.4 years (range: 19–86 years), and 50 (47.6%) were male. The mean age and mean PTA thresholds at all frequencies (measured at 250, 500, 1,000, 2,000, 3,000, 4,000, and 8,000 Hz bilaterally) showed no statistically significant differences between the HL-T and HL-NT groups (Table 1). Individuals with otologic disorders such as otosclerosis and Meniere's disease, chronic headache, psychiatric or neurological disorders, current psychotropic/central nervous system-active medications, history of drug/alcohol abuse, and/or a history of head injury (with loss of

TABLE 1 Demographic and audiological characteristics of the study subjects

	HL-T group	HL-NT group	*p*-value
Number of subjects	65	104	
Male:Female	21:44	50:54	
Mean age	66.6 ± 10.1	67.5 ± 13.4	.631
Mean PTA threshold			
Right			
250 Hz	29.1 ± 9.1	29.2 ± 11.8	.930
500 Hz	32.4 ± 9.1	35.5 ± 11.4	.070
1,000 Hz	39.9 ± 8.4	41.9 ± 11.1	.237
2,000 Hz	44.7 ± 8.4	46.8 ± 11.7	.213
3,000 Hz	51.4 ± 9.1	53.1 ± 14.1	.398
4,000 Hz	57.1 ± 8.5	58.7 ± 15.1	.426
8,000 Hz	69.5 ± 11.3	71.6 ± 18.2	.392
Left			
250 Hz	30.5 ± 10.0	30.2 ± 13.9	.905
500 Hz	34.7 ± 9.3	36.4 ± 12.8	.368
1,000 Hz	40.8 ± 8.4	43.0 ± 12.2	.200
2,000 Hz	45.6 ± 8.6	47.8 ± 13.3	.247
3,000 Hz	52.0 ± 7.3	54.1 ± 15.5	.321
4,000 Hz	57.9 ± 8.2	60.0 ± 17.6	.378
8,000 Hz	70.1 ± 10.5	71.7 ± 18.5	.692

Abbreviations: HL-NT, hearing loss without tinnitus; HL-T, hearing loss with tinnitus.

consciousness) or seizures were excluded from the study to ensure a homogeneous sample. The data that support the findings of this study are available from the corresponding author upon reasonable request.

2.2 | EEG recording

The EEG recordings were performed in accordance with a standard diagnostic and neuromodulation treatment protocol after obtaining informed consent. Participants refrained from alcohol consumption for 24 hr before EEG recording, and from caffeinated beverages on the day of recording, to prevent alcohol-related changes in the EEG (Vanneste & De Ridder, 2012) and a caffeine-induced decrease in alpha waves, respectively (Barry, Clarke, & Johnstone, 2011; Foxe et al., 2012).

Each participant sat upright on a comfortable chair in a well-lit room that was shielded against sound and stray electric fields. Then, EEG recordings were obtained for ~5 min using a tin electrode cap (ElectroCap, Eaton, OH) and Mitsar EEG-201 amplifier (Mitsar, St. Petersburg, Russia). The vigilance of the participants was determined according to EEG parameters such as the appearance of spindles or slowing of the alpha rhythm, where enhanced theta power reflects drowsiness (Moazami-Goudarzi, Michels, Weisz, & Jeanmonod, 2010). The EEG was recorded with 19 electrodes using the International 10–20 system and referenced to linked ears; the impedance of all electrodes was kept below 5 kΩ during EEG recording. Data were collected under eyes-closed conditions (sampling rate, 1,024 Hz; bandpass, 0.15–200 Hz), using WinEEG software (version 2.84.44; Mitsar). The data were resampled to 128 Hz, band-pass filtered (fast Fourier transform filter) to 2–44 Hz, and transposed into Eureka! Software (Sherlin & Congedo, 2005). Then, the data were plotted and carefully inspected for manual artifact rejection. All episodic artifacts, such as eye movements, eye blinks, body movement, teeth clenching, and electrocardiogram artifacts, were removed from the EEG signals. An independent component analysis (ICA) was also performed to confirm that all artifacts had been removed. The power spectra were compared (a) after visual artifact rejection only, and (b) after visual artifact and ICA component rejection. There was no statistically significant difference in the mean power of the delta (2–3.5 Hz), theta (4–7.5 Hz), alpha1 (8–10 Hz), alpha2 (10–12 Hz), beta 1 (13–18 Hz), beta2 (18.5–21 Hz), beta 3 (21.5–30 Hz), or gamma (30.5–44 Hz) frequency band (Han et al., 2018; Kim et al., 2016; Lee et al., 2019; Lee, Choi, Koo, De Ridder, & Song, 2020; Song et al., 2017; Vanneste, Song, & De Ridder, 2018) between the two approaches. Therefore, we reported the results of the two-step artifact correction data. Average Fourier cross-spectral matrices were computed for the aforementioned bands from delta to gamma.

2.3 | Metric graph

The brain network of 84 Brodmann areas (BAs; Table 2), and the corresponding lagged phase coherence between all pairs of Bas, represent a fully connected undirected metric graph with 84 nodes and $(84¦2) = 3{,}486$ undirected edges with defined lengths (Mohan, De Ridder, & Vanneste, 2016). Weighted and binary graph models have been widely used for analyzing the brain network (Mohan et al., 2016). As our focus was primarily on geometric properties, we modeled the brain network using a connected metric graph whose nodes are 84 BAs. Analogous to the relationship between conductance and resistance, we defined the length of an edge as the multiplicative inverse of its lagged phase coherence (Newman, 2001). The metric induced on the metric graph is the path metric, defined as the infimum of the lengths of the paths between two given points.

2.4 | Volume entropy

Let v be a connected finite metric graph without any terminal node, which is not a cycle. Denote $l(f)$ by the length of the edge f. The length of an edge path $e_1e_2\cdots e_n$ in X is defined by $l(e_1e_2\cdots e_n) = l(e_1) + l(e_2) + \cdots + l(e_n)$.

The volume entropy h_{vol} of metric graph X is characterized by the limit of the exponential growth rate of the number of edge paths in X of length less than r as $r \to \infty$, that is,

TABLE 2 All the Brodmann areas included in the study

Brodmann areas	Abbreviation	Name of the Brodmann area
BA01	S1	Primary somatosensory cortex
BA02	S2	Secondary somatosensory cortex
BA03	S3	Tertiary somatosensory cortex
BA04	M1	Primary motor cortex
BA05	SPS	Superior parietal sulcus
BA06	SMA	Supplementary motor area
BA07	SPG	Superior parietal gyrus
BA08	Pre-SMA	Pre-supplementary motor area
BA09	DLPFC	Dorsolateral prefrontal cortex
BA10	FPC	Fronto-polar cortex
BA11	OFC	Orbital frontal cortex
BA13	Insula	Insula
BA17	V1	Primary visual cortex
BA18	V2	Secondary visual cortex
BA19	Cuneus	Cuneus
BA20	ITG	Inferior temporal gyrus
BA21	MTG	Medial temporal gyrus
BA22	STG	Superior temporal gyrus
BA23	PCC1	Posterior cingulate cortex1
BA24	dACC	Dorsal anterior cingulate cortex
BA25	sgACC	Subgenual anterior cingulate cortex
BA27	PHC1	Parahippocampal gyrus1
BA28	HIP1	Hippocampal area1
BA29	RSC1	Retrosplenial cortex1
BA30	RSC2	Retrosplenial cortex2
BA31	PCC2	Posterior cingulate cortex2
BA32	prACC	Pregenual anterior cingulate cortex
BA33	rACC	Rostral anterior cingulate cortex
BA34	HIP	Hippocampus
BA35	HIP2	Hippocampal area2
BA36	PHC2	Parahippocampal gyrus2
BA37	OTC	Occipital-temporal cortex
BA38	TP	Temporal pole
BA39	AG	Angular gyrus
BA40	IPS	Intra-parietal sulcus
BA41	A1	Primary auditory cortex
BA42	A2	Secondary auditory cortex
BA43	PCG	Postcentral gyrus
BA44	OPCG	Opercular part of inferior frontal gyrus
BA45	IFG	Inferior frontal gyrus
BA46	MPFC	Medial prefrontal cortex
BA47	VLPFC	Ventrolateral prefrontal cortex

$$h_{\mathrm{vol}} = \lim_{r\to\infty} \frac{\log N_r(x_0)}{r},$$

where x_0 is a fixed node in X and $N_r(x_0)$ is the number of edge paths $e_1e_2\cdots e_n$ in X, starting from x_0 without backtracking, such that $l(e_1e_2\cdots e_{n-1}) < r \le l(e_1e_2\cdots e_n)$. It is known that the limit exists and volume entropy is independent of the node x_0. In other words, if $N_r(x_0)$ is asymptotic to e^{hr}, then h is the volume entropy.

To compute the volume entropy h_{vol} algorithmically, we defined a matrix $L(h) \in M_{|EX|\times|EX|}(\mathbb{R})$ for the metric graph X as

$$[L(h)]_{ef} = \begin{cases} e^{-hl(f)} \text{ if } t(e) = i(f), i(e) \neq t(f) \\ 0 \quad \text{otherwise} \end{cases},$$

where EX is the set of directed edges in graph X, $t(e)$ is the terminal node of e, and $i(f)$ is the initial node of f. The volume entropy is the unique positive constant h such that the largest absolute value of the eigenvalue of $L(h)$ equals 1 (Lim, 2008).

2.5 | Afferent node capacity

For the eigenvector $x = (x_e)_{e\in EX} \in R^{|EX|}$ of $L(h_{\mathrm{vol}})$ associated with volume entropy h_{vol}, each component x_e corresponding to the directed edge $e \in EX$ is the edge capacity on e. The edge capacity represents how the edge affects the spread of information. Distinct directed edges with the same terminal nodes have similar edge capacities. This property is specific to brain networks because they are complete graphs in which every two nodes are connected by an edge. This tendency becomes stronger as the number and degree of nodes increase. By summing the edge capacities of directed edges with the same terminal nodes, we converted the capacities of directed edges to those of nodes. Consequently, we obtained a vector indexed by nodes, that is, functional data on brain regions; we refer to this as the afferent node capacity. One may consider the efferent node capacity by summing the edge capacity over the edges with the same initial node. However, the value of the efferent node capacity is not a good characteristic of the node. If we regard the number of paths with length of at most T to correspond to the amount of information spreading out up to time T, volume entropy measures asymptotically (as T goes to infinity) how well information spreads along the edges of a graph for sufficiently large T. In this regard, volume entropy plays a role as a global network measure. When edge paths pass through a node more frequently, the afferent node capacity at the node is larger. For an alternative method to convert weights on edges to weights on nodes, please refer to our recent study (Lee, Kim, et al., 2019).

2.6 | Statistical analysis

We performed a permutation test (Wasserman, 2013) to assess the difference in afferent node capacity between the two groups for each

node (region of interest; ROI) of each frequency band. Because our data set is not large enough to be approximated to a normal distribution, commonly used statistical test methods are not desirable; thus, we used a permutation test, which is considered the most useful test for small samples. Under the hypothesis that the two samples are identically distributed, we tested the difference in average afferent node capacity between the two groups. The permutation was repeated 100,000 times for comparing volume entropy and afferent node capacity between the HL-T and HL-NT groups.

Because afferent node capacity is the sum of all edge capacities, where the edge capacity depends on both the initial and terminal node, the afferent node capacity of the two nodes x and y may differ significantly, mainly due to a difference in the capacity of a few edges of terminal nodes x and y, respectively. To identify the edge capacity distribution, we compared the average edge capacity between the HL-T and HL-NT groups and performed the permutation test with 10,000 repetitions.

Statistical analysis was performed using Python (version 3.7.0). In all analyses, $p < .01$ was taken to indicate statistical significance.

3 | RESULTS

3.1 | Comparison of volume entropy between the HL-T and HL-NT groups

The statistical analysis gives no significant difference between the HL-T and HL-NT groups in terms of volume entropy for any frequency bands. The distributions of volume entropy in the HL-T and HL-NT groups are in Figure 1.

From the result of the statistical analysis, we may assume that the networks in the HL-T and HL-NT groups are well-normalized, that is, the distributions of the global measure (volume entropy) between two groups are not statistically different. Based on the assumption, comparing the afferent node capacities, which are highly related to the volume entropy, is more meaningful than not normalized case.

3.2 | Comparison of afferent node capacity between the HL-T and HL-NT groups

Figure 2 depicts the afferent node capacity distribution of the 84 BAs for all eight frequency bands. Figure 3 illustrates the relative afferent node capacity of the HL-T and HL-NT groups. As summarized in Table 3, the HL-T and HL-NT groups showed statistically significant differences in afferent node capacity for a total of 14 ROIs for the theta, alpha2, and beta3 frequency bands. For these 14 ROIs, the afferent node capacity is summarized in Figure 3.

As illustrated in Figure 4 and summarized in Table 3, the HL-T group showed a significantly higher afferent node capacity in the left orbitofrontal cortex (OFC; $p < .01$), left subgenual anterior cingulate cortex (sgACC; $p < .01$), and left ventrolateral prefrontal cortex (VLPFC; $p < .01$) compared with the HL-NT group for the theta frequency band. By contrast, the mean afferent node capacity at the right medial temporal gyrus (medTG) for the theta frequency band was significantly higher in the HL-NT group compared with the HL-T group ($p < .01$) (Figure 5, upper panel).

For the alpha2 frequency band, the afferent node capacity in the left opercular part of the inferior frontal gyrus (OPCG; $p < .01$) and left

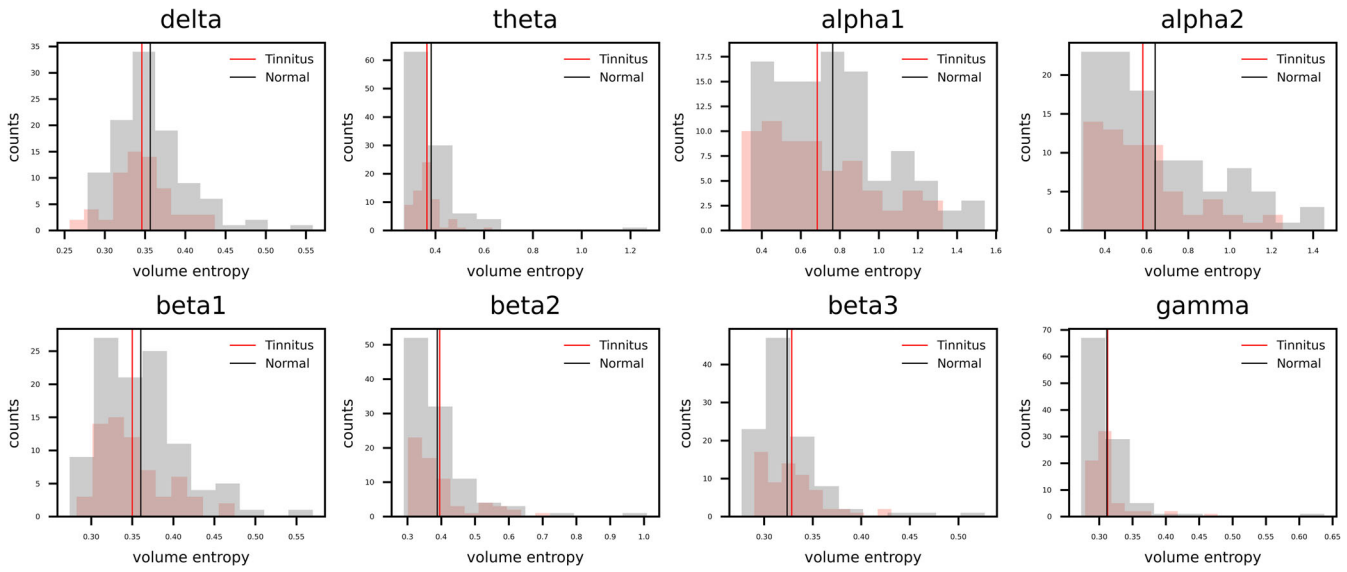

FIGURE 1 Histogram of volume entropy. The histograms show the distribution of volume entropy on various frequency bands in the HL-T (red) and HL-NT (black) groups. The red vertical line means the average of volume entropy in the HL-T group and the black vertical line means the average of volume entropy in the HL-NT group

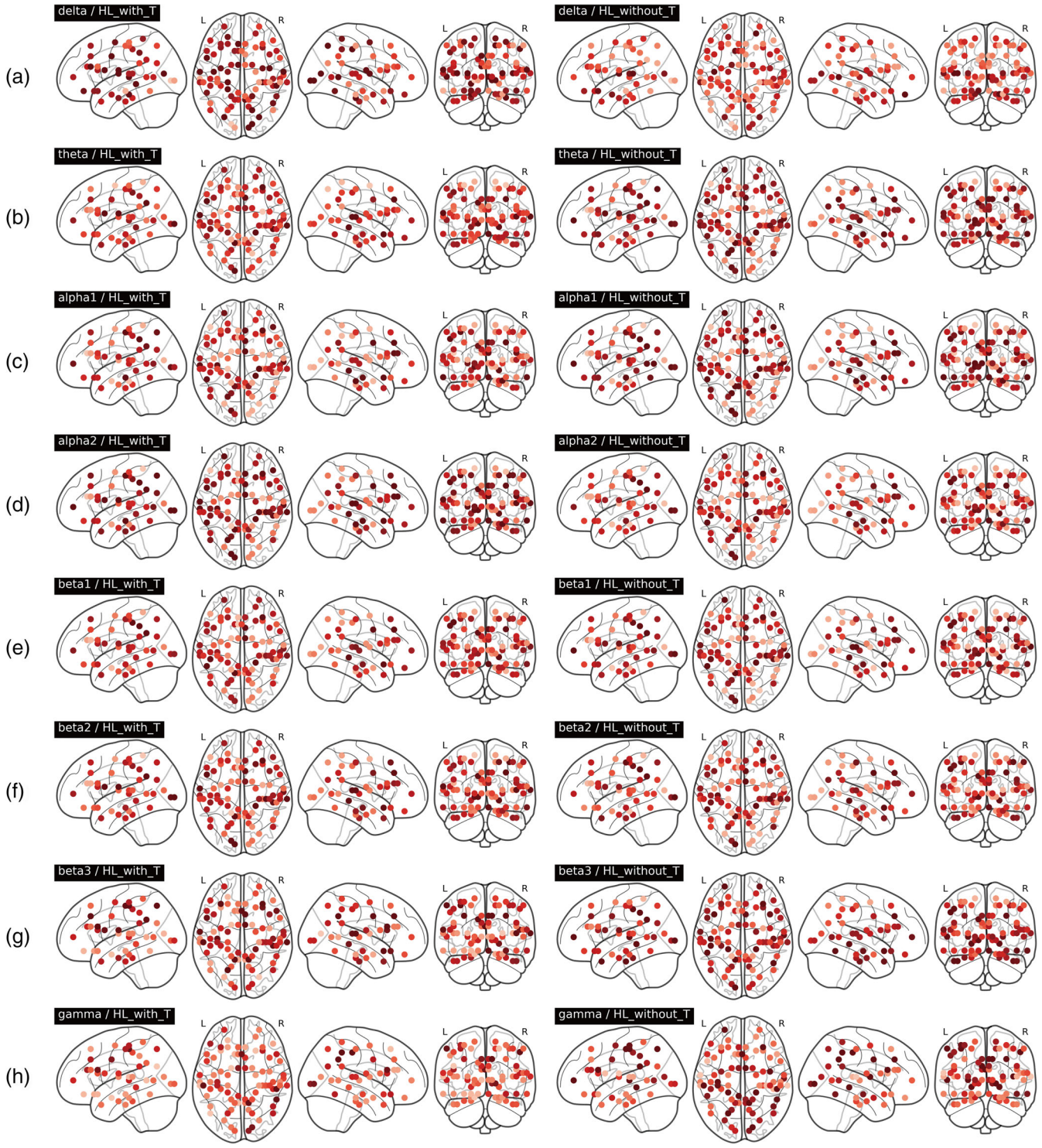

FIGURE 2 Distribution of afferent node capacities on the Brodmann areas. (a)–(i) represent the distribution of afferent node capacities on the 84 Brodmann areas in left: HL-T and right: HL-NT groups in (a) delta, (b) theta, (c) alpha1, (d) alpha2, (e) beta1, (f) beta2, (g) beta3, and (h) gamma frequency band. The figures have been drawn using Python nilearn package (Version 0.2.5)

inferior frontal gyrus (IFG) ($p < .01$) was significantly higher in the HL-T group compared with the HL-NT group. By contrast, the afferent node capacity in left retrosplenial cortex 1 (RSC1; $p < .01$), right posterior cingulate cortex 1 (PCC1; $p < .01$), and right RSC1 ($p < .01$) was significantly higher in the HL-NT group compared with the HL-T group (Figure 5, middle panel).

For the beta3 frequency band, the afferent node capacity in the right insula ($p < .01$), right hippocampus ($p < .01$), right hippocampal

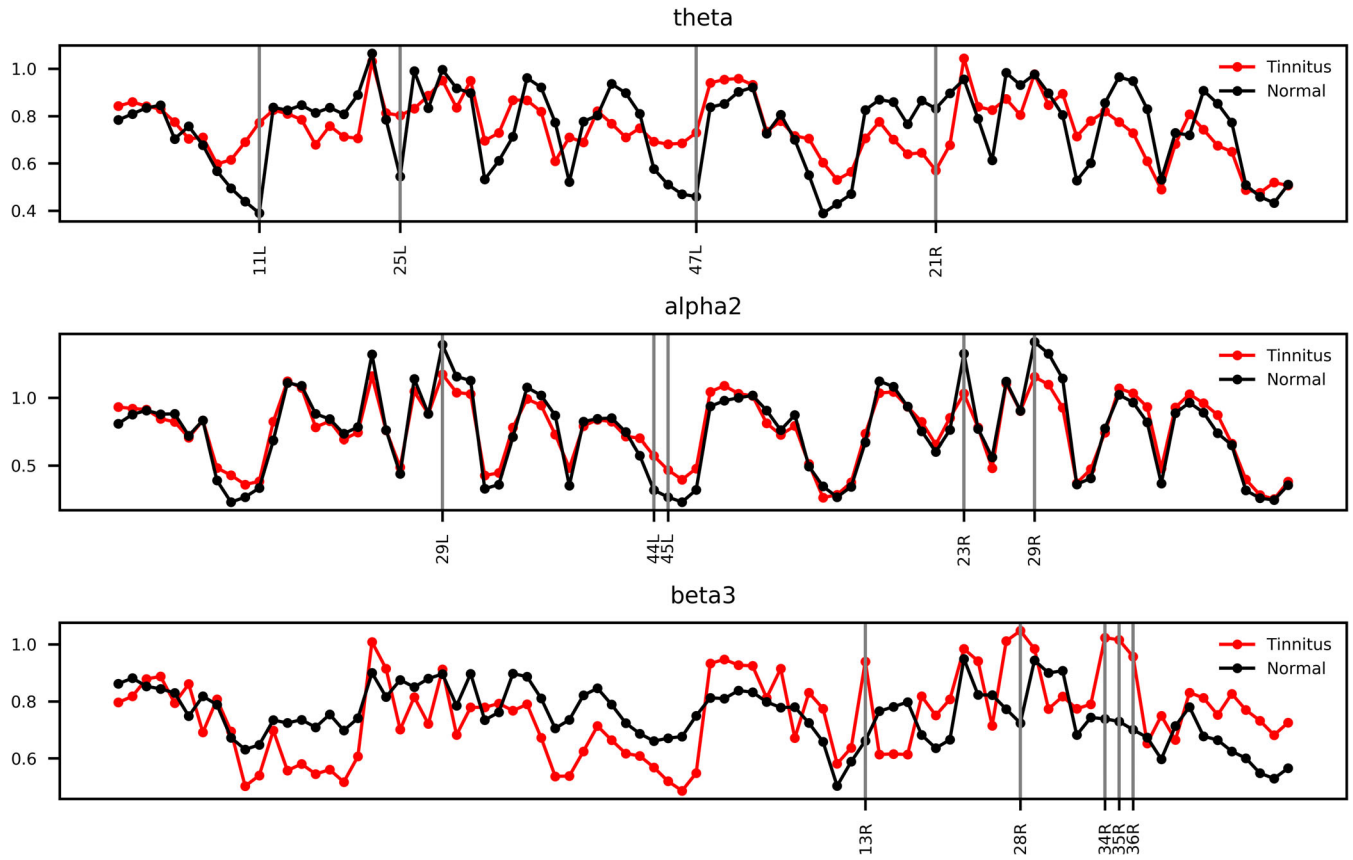

FIGURE 3 Afferent node capacity for the two groups. Average of afferent node capacities on each Brodmann area are calculated in the HL-T (red) and HL-NT (black) groups in upper: theta, middle: alpha2 and bottom: beta3 frequency band. The gray vertical lines on the significantly different Brodmann areas. Any other frequency bands have no significantly different Brodmann areas

TABLE 3 Result of statistical inference with significant level 0.01

Frequency band	Abbreviation	BA	*p*-value	Tinnitus	Non-tinnitus
Theta	OFC	11L	.00003	0.77201489	0.38964517
	sgACC	25L	.00741	0.8021413	0.54459024
	VLPFC	47L	.00388	0.72965909	0.46009869
	MTG	21R	.00671	0.57059879	0.83148991
Alpha2	RSC1	29L	.00941	1.17301991	1.39255565
	OPCG	44L	.00214	0.57080755	0.31750684
	IFG	45L	.00833	0.4669897	0.26588954
	PCC1	23R	.00125	1.03064385	1.3262293
	RSC1	29R	.00535	1.15502661	1.41378237
Beta3	Insula	13R	.00853	0.93953276	0.66183085
	HIP1	28R	.00117	1.04740913	0.72378116
	HIP	34R	.00648	1.0233051	0.73847828
	HIP2	35R	.00317	1.01532414	0.72952998
	PHC2	36R	.00697	0.95658985	0.70022195

Note: Tinnitus, an average of afferent node capacity on the ROI in the tinnitus group; Non-tinnitus, an average of afferent node capacity on the ROI in the non-tinnitus group.

area (HIP) 1 ($p < .01$), right HIP2 ($p < .01$), and right parahippocampal gyrus (PHC) 2 ($p < .01$) was significantly higher in the HL-T group compared with the HL-NT group (Figure 5, lower panel).

For the delta, alpha1, beta1, beta2, and gamma frequency bands, no significant difference was observed between the HL-T and HL-NT groups in terms of afferent node capacity for any of the 84 ROIs.

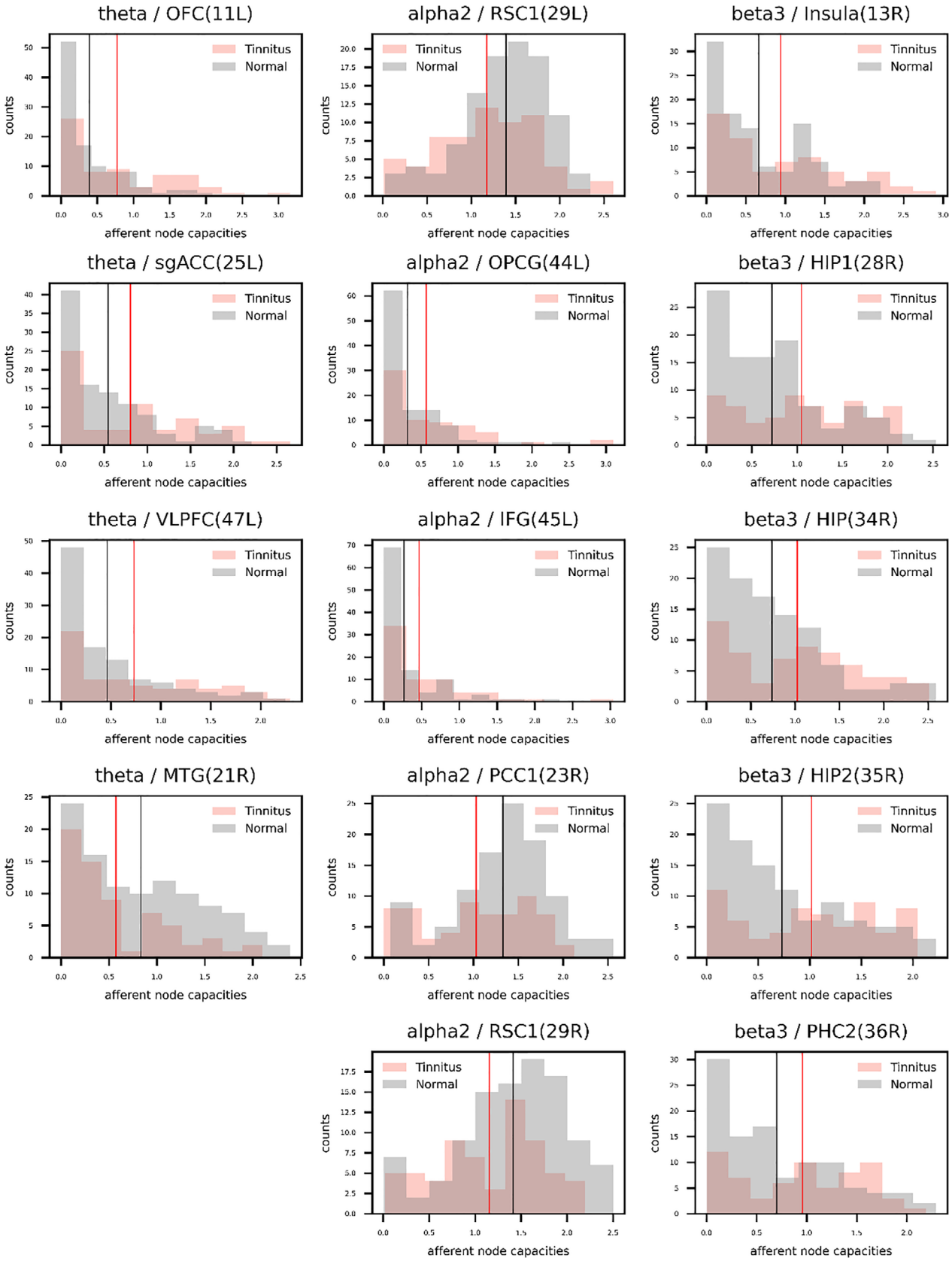

FIGURE 4 Histogram of afferent node capacity. The histograms show the distribution of afferent node capacity on significantly different (frequency band)/(Brodmann area) pairs in the HL-T (red) and HL-NT (black) groups. The red vertical line means the average of afferent node capacities in the HL-T group and the black vertical line means the average of afferent node capacities in the HL-NT group

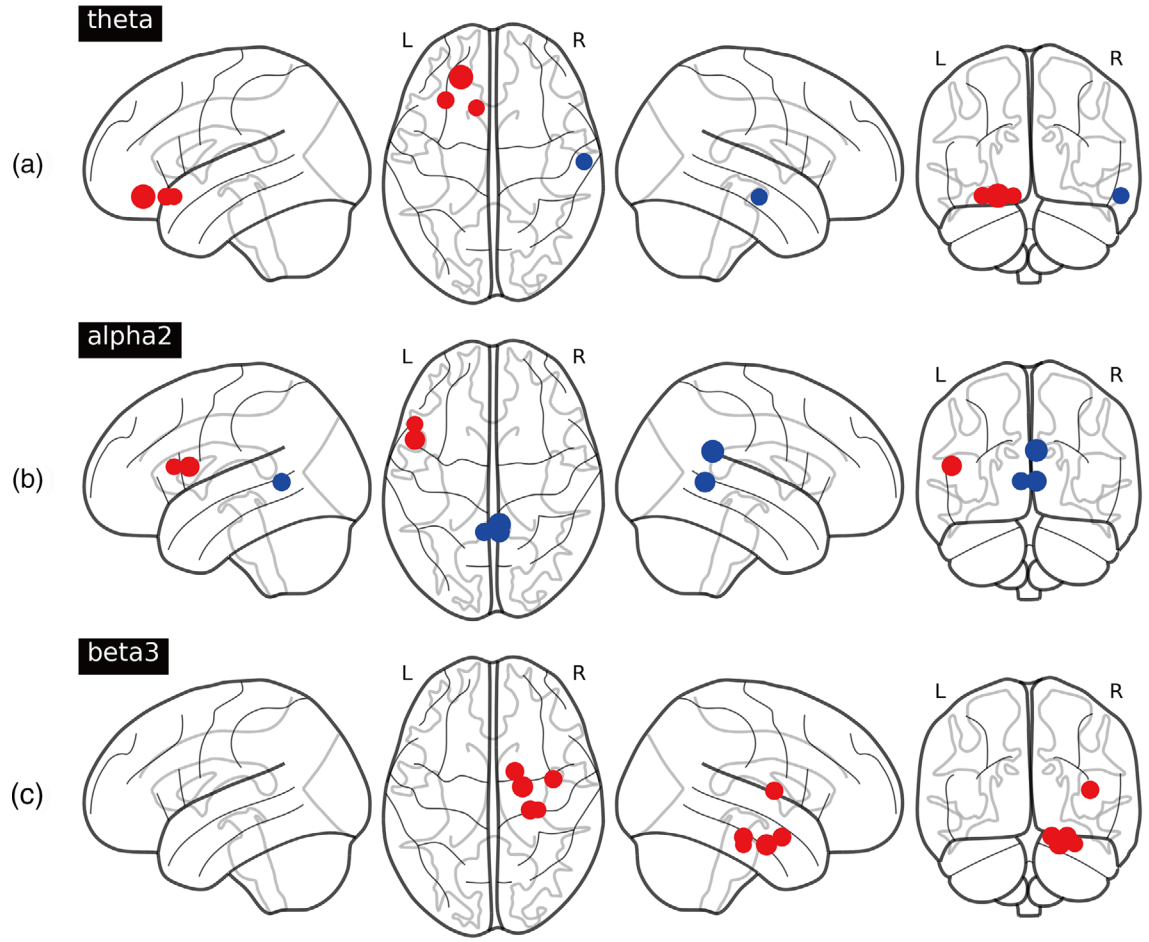

FIGURE 5 Significantly different BAs. The pointed regions indicate significantly different BAs in the (a) theta, (b) alpha2, and (c) beta3 frequency bands. Dot size indicates the extent of the difference in afferent node capacity between the two groups for corresponding BAs. At the red point, the average afferent node capacity in the HL-T group is greater than that in the HL-NT group; the opposite is true at the blue point. (a) Left orbitofrontal cortex (OFC), left subgenual anterior cingulate cortex (sgACC), left ventrolateral prefrontal cortex (VLPFC), and right medial temporal gyrus (medTG). (b) Left retrosplenial cortex 1 (RSC1), left opercular part of the inferior frontal gyrus (OPCG), left inferior frontal gyrus (IFG), right posterior cingulate cortex 1 (PCC1), and right RSC1. (c) Right insula, right hippocampal area (HIP) 1, right HIP, right HIP2, and right parahippocampal gyrus (PHC) 2. Figures were illustrated using the nilearn Python package (version 0.2.5)

3.3 | Comparison of edge capacity between the HL-T and HL-NT groups

In Figure 6, for a fixed ROI, the edge capacities of all of directed edges showing significant differences in the theta, alpha2, and beta3 frequency bands are colored. The edge capacities of all the directed edges were higher (lower) if the corresponding node had a higher (lower) afferent node capacity.

For an edge capacity $x = (x_e)_{e \in EX} \in R^{|EX|}$, we transformed x to a square matrix M as $[M]_{vw} = x_{\overrightarrow{vw}}$ and performed a permutation test (< 0.01) for each component (Figure 7). Each column of M is a set of directed edges with the same terminal node. Figure 7 shows that the columns of M with significantly different components were distributed vertically, indicating that most of the directed edges whose terminal node exhibited a significant difference in afferent node capacity also had a significant difference in edge capacity.

For the theta frequency band, the columns with significantly different components were in the left frontoparietal cortex (FPC), left OFC, left sgACC, left VLPFC, and right dorsolateral prefrontal cortex (DLPFC). For the alpha2 frequency band, the columns with significantly different components were in the right DLPFC, left RSC1, left OPCG, left IFG, right PCC1, and right RSC1. For the beta3 frequency band, the columns with significantly different components were in the right insula, right HIP, right HIP1, right HIP2, and right PHC2. For the delta, alpha1, beta1, beta2, and gamma frequency bands, no significant differences were observed between the HL-T and HL-NT groups with respect to edge capacity values.

4 | DISCUSSION

In the present study, we compared HL-T and HL-NT groups, in terms of the afferent node capacity of 84 ROIs in the brain, via lagged linear

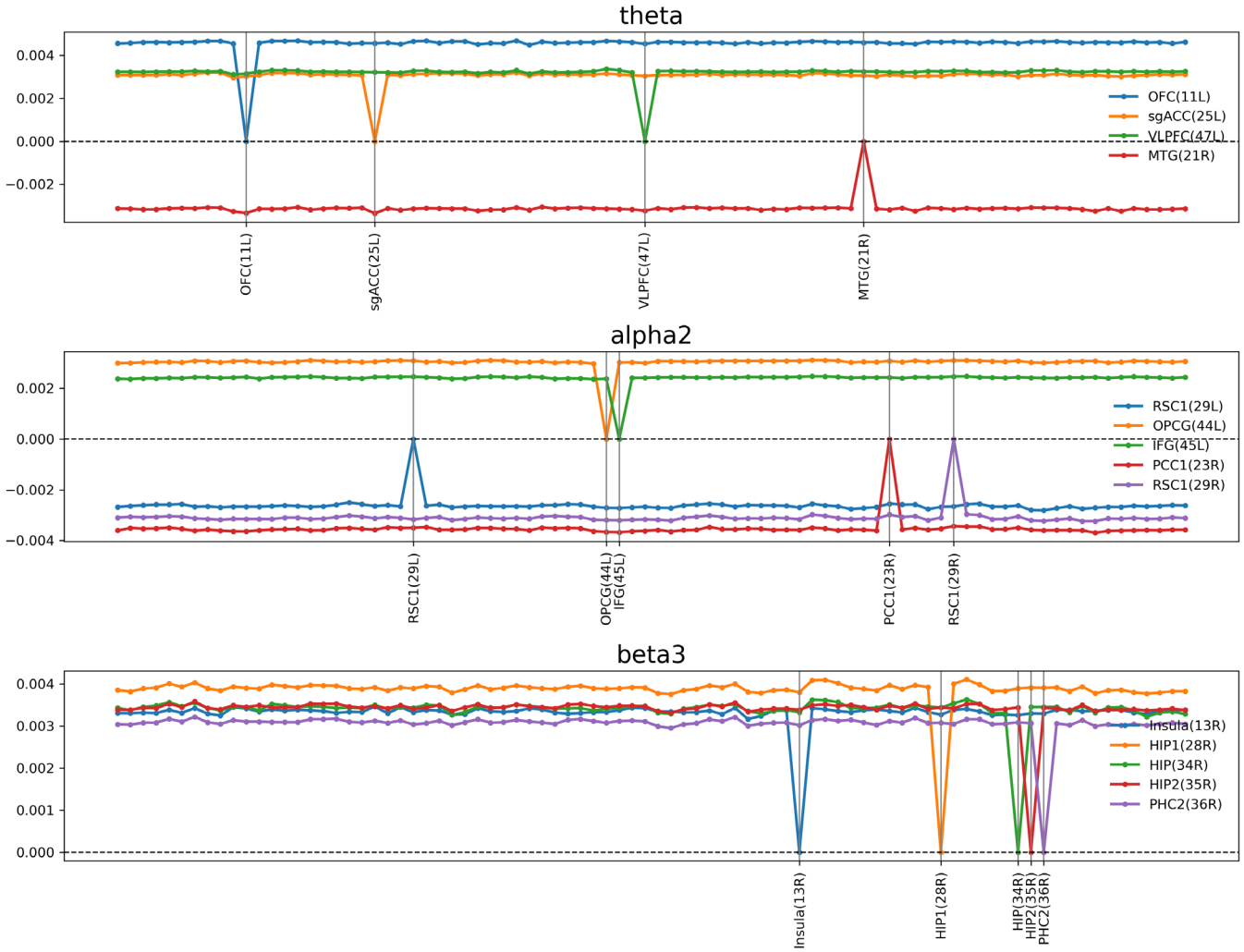

FIGURE 6 Difference in edge capacity between the two groups. The lines represent the difference in edge capacity between the two groups in the (a) theta, (b) alpha2, and (c) beta3 frequency bands. The outer circle corresponds to 84 ROIs and the lines in each figure are significantly different directed edges in the white-marked ROI. The red line indicates that the average edge capacity in the HL-T group is greater than that in the HL-NT group; the blue line indicates the opposite. Figures were illustrated using the mne Python package (version 0.20.5)

connectivity analysis of eight rs-qEEG frequency bands. The HL-T group showed significantly higher afferent node capacity in the left OFC, left sgACC, and left VLPFC compared with the HL-NT group for the theta frequency band, while the HL-NT group had a significantly higher afferent node capacity in the right medTG compared with the HL-T group. For the alpha2 frequency band, the HL-T group had a significantly higher afferent node capacity in the left IFG ($p < .01$) compared with the HL-NT group, while the HL-NT group showed significantly higher values in the bilateral RSC1 and right PCC1 compared with the HL-T group. For the beta3 frequency band, the HL-T group showed a significantly higher afferent node capacity in the right insula, right hippocampus, and parahippocampus compared with the HL-NT group. Thus, the HL-T and HL-NT groups showed marked differences in the spread of neural information among many cortical areas for different frequency bands.

As summarized above, the HL-T group had a significantly higher afferent node capacity in the right hippocampus and parahippocampus compared with the HL-NT group for the beta3 frequency band. The HL-NT group also showed higher afferent node capacity in the bilateral RSC1 for the alpha2 frequency band. Considering that an increase in qEEG alpha waves reflects top-down, inhibitory control processes (Axelsson & Ringdahl, 1989), the relatively increased afferent node capacity in the bilateral RSC1 for the alpha2 frequency band in the HL-NT group may reflect relatively decreased inhibitory control processes in the bilateral RSC1.

It has been suggested that tinnitus is the result of Bayesian inference, and may be generated to reduce perceptual uncertainty (De Ridder, Joos, & Vanneste, 2014; De Ridder, Vanneste, & Freeman, 2014). The Bayesian brain can be conceptualized as a probability machine that constantly makes predictions based on its model of the world, and then updates these predictions by active exploration of the environment via the senses (Friston, 2010), to reduce the uncertainty that is inherent to a changing environment (De Ridder, Vanneste, & Freeman, 2014). Against this background, sensory

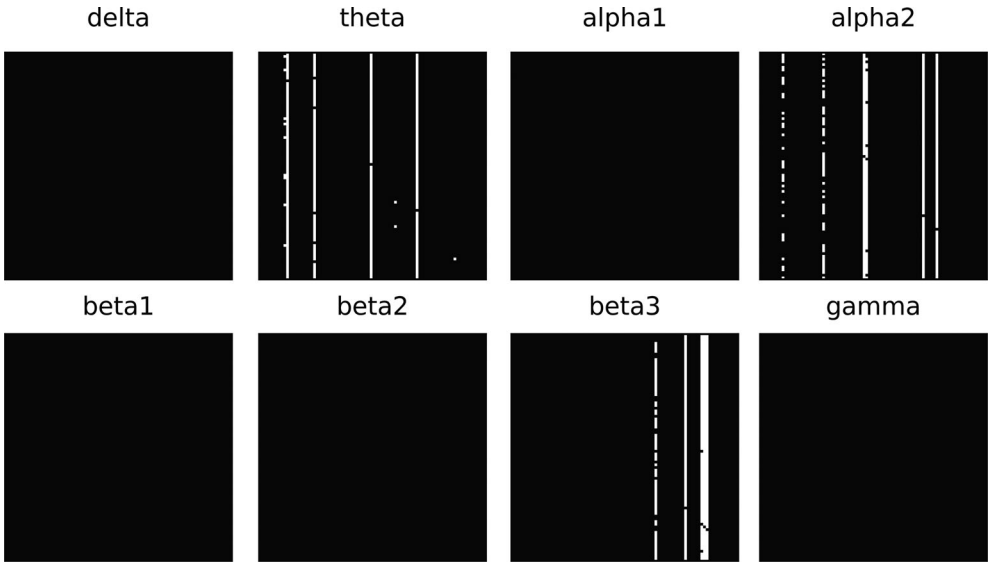

FIGURE 7 Significantly different directed edges. The components of square matrices that are significantly different between the HL-T and HL-NT groups are white; those that are not significantly different are black. The theta band has columns containing white points in the left frontoparietal cortex (FPC), left OFC, left sgACC, left VLPFC, right dorsolateral prefrontal cortex (DLPFC), right MTG, and right PHC2. The alpha2 band has columns containing white points in the left DLPFC, left RSC1, left OPCG, left IFG, right PCC1, and right RSC1. The beta3 band has columns containing white points in the right insula, right HIP1, right HIP, right HIP2, and right PHC2

perception can be viewed as the result of memory-based predictions that are verified and updated with additional sensory input. If sensory input is not available, for example, due to HL, then the missing auditory information can be retrieved from memory (De Ridder, Joos, & Vanneste, 2014; De Ridder, Vanneste, & Freeman, 2014). The model of the world maintained by the brain can be described as a cognitive map stored in the hippocampal-parahippocampal area and OFC (Wikenheiser & Schoenbaum, 2016). A cognitive map can be defined as an abstract map of causal relationships, that is, a set of mental representations that binds external sensory features (hippocampus/parahippocampus) with internal motivational or emotional factors (OFC) to form an integrated relational database.(Tolman, 1948; Wikenheiser & Schoenbaum, 2016) These same areas are involved in predictions of sensory stimuli to reduce perceptual uncertainty (Weilnhammer, Stuke, Sterzer, & Schmack, 2018). The updating of sensory predictions involves a cascade from early unisensory encoding in primary sensory cortices to reliability-weighted fusion in parietal–temporal cortices, and then to causal inference (primarily in the OFC) of behaviorally relevant (insula) signals (Cao, Summerfield, Park, Giordano, & Kayser, 2019). The VLPFC suppresses behaviorally irrelevant sensory stimuli in a cross-modal context to minimize perceptual bias (Cao et al., 2019).

The findings of this study can be interpreted in the context of the Bayesian brain to derive a model for tinnitus (De Ridder, Joos, & Vanneste, 2014; De Ridder, Vanneste, & Freeman, 2014; Hullfish, Sedley, & Vanneste, 2019; Lee et al., 2017; Vanneste & De Ridder, 2016). Some individuals with HL develop tinnitus, which is characterized by increased information transmission efficiency in a network that comprises the lateral OFC, VLPFC, sgACC, and parahippocampal and hippocampal areas, as well as the insula.

The parahippocampus is involved in auditory memory and thus may also play a role in the generation of tinnitus in cases of HL (De Ridder et al., 2006; De Ridder, Elgoyhen, Romo, & Langguth, 2011). Indeed, parahippocampal activity was more common in tinnitus subjects compared with non-tinnitus controls in a recent connectomics study (Mohan et al., 2016). Transient suppression of hippocampal activity by amytal injections into the anterior choroidal artery could also suppress tinnitus (De Ridder et al., 2006). Furthermore, in a recent study describing partial peripheral reafferentation via the use of a hearing aid in tinnitus subjects, pre-hearing aid parahippocampal activity was shown to be a negative prognostic factor for tinnitus improvement (Han et al., 2020).

The parahippocampus has been suggested to act as a gatekeeper to the hippocampus, filtering out irrelevant or redundant auditory input (Boutros et al., 2008; Tulving & Markowitsch, 1997). In a recent proof-of-concept study, tinnitus patients with marked HL exhibited increased parahippocampal activity compared with healthy controls; moreover, the range of HL correlated with changes in cortical activity in the parahippocampus (Vanneste & De Ridder, 2016). In another recent study, subjects with HL-T showed increased functional connectivity between the parahippocampus and auditory cortex compared with subjects with HL-NT (Vanneste, Alsalman, & De Ridder, 2019). Based on this literature and a recent Bayesian brain model explaining the generation of tinnitus in terms of Bayesian updating of missing auditory information (and thus the generation of phantom auditory perception) (De Ridder, Vanneste, & Freeman, 2014), we surmise that, when opened, a "parahippocampal sensory gate" generates phantom sounds from auditory memories stored in the hippocampus, to compensate for missing auditory information due to HL. The posterior hippocampus/parahippocampus contains a cognitive map of the causal

relationships between sensory inputs in space and time (Wikenheiser & Schoenbaum, 2016). This is also consistent with studies on the neural correlates of "multisensory inference" (Weilnhammer et al., 2018). The significantly higher afferent node capacity of the (para)hippocampal area in our HL-T group suggests a crucial role of the parahippocampus in the generation of tinnitus, by promoting the spread of stored auditory information to other cortical areas. However, this compensatory generation of phantom auditory perception by the parahippocampus does not occur in all subjects with HL: unnecessary retrieval of parahippocampal auditory memory may be contingent upon interactions with other cortical areas. The OFC also contains a cognitive map of the world; however, it is based on behavioral relevance rather than contextual multisensory input (Wikenheiser & Schoenbaum, 2016). This suggests that for individuals who develop tinnitus, the missing auditory information is deemed salient by the parahippocampus, which drives it to distribute the missing auditory input across the brain. Previous studies have suggested that the insula, especially the anterior insula, engages in mathematical tasks, that is, the tracking of risk and risk prediction errors (Boorman, Behrens, Woolrich, & Rushworth, 2009; Bossaerts, 2010). In addition, activation of the insula due to a perceived threat or risk prediction error has been found to be closely related to activation of the ACC or IFG (Christopoulos, Tobler, Bossaerts, Dolan, & Schultz, 2009). This is not surprising, as the insula is part of the salience network (SN) in charge of salience processing and executive control (Seeley et al., 2007). Therefore, we speculate that, in our HL-T group, decreased peripheral auditory input may have been regarded as a behaviorally salient stimulus by the insula, which may promote the generation of tinnitus by pulling auditory memories from the (para) hippocampus and aforementioned prefrontal areas. Also, as the IFG is a part of the central executive network (CEN) that is related to activity inhibition, emotion, and working memory (Lan et al., 2021), the modulatory role of the SN with regard to the function of the CEN may have resulted in better perception of the parahippocampal memory-based tinnitus. Salience is also related to the subjective value that the brain (sgACC) ascribes to missing information, irrespective of the stimulus type, as demonstrated by a meta-analysis (Clithero & Rangel, 2014). Furthermore, the sgACC and parahippocampal area are part of a general network processing aversive/unpleasant stimuli (Moulton et al., 2011), which is also present in tinnitus (Joos, Vanneste, & De Ridder, 2012; Vanneste & De Ridder, 2015a) The VLPFC forms part of a Bayesian inference model of the suppression of irrelevant sensory information (Cao et al., 2019). In a broader sense, the VLPFC suppresses the "silent" model of the world and generates a new model that encompasses tinnitus (Donoso, Collins, & Koechlin, 2014).

In summary, in the presence of HL, a highly activated network (measured by afferent node capacity) consisting of the OFC, sgACC, and VLPFC, in which Bayesian inferences related to decreased peripheral auditory input generate tinnitus by retrieving stored auditory memories from the (para)hippocampus, generates a model of the world incorporating tinnitus because the brain considers the missing auditory input behaviorally relevant. By contrast, the HL-NT group showed significantly higher afferent node capacity in the right PCC1 and right medTG for the alpha2 and theta frequency bands, respectively, compared with the HL-T group. The PCC is a core component of the DMN, which shows a high rate of metabolism in healthy subjects not focused on the outside world, and decreases in activity across a range of cognitive loads (Raichle et al., 2001; Shulman et al., 1997). The PCC has long been regarded as a posterior hub of the DMN (Fox et al., 2017; Xu, Yuan, & Lei, 2016) and has recently been suggested to regulate the DMN (Wang, Chang, Chuang, & Liu, 2019). Whether a new model of the world is required depends on the current needs, behavioral flexibility, and prior knowledge about the environment of a given individual (Pearson, Heilbronner, Barack, Hayden, & Platt, 2011). Based on Bayesian inference, the PCC is involved in detecting sensory changes and drives subsequent shifts in self-referential processing and thus behavior (Pearson et al., 2011). The PCC is also the main cortical hub of the parasympathetic and digestive systems (Beissner, Meissner, Bar, & Napadow, 2013). The PCC does not consider a decrease in auditory input salient. The MedTG has been suggested as a component of the DMN (Murphy et al., 2018), and microstate analysis suggested that it is an important component of a "tinnitus generating network" (Vanneste et al., 2019). The MedTG is involved in updating auditory predictions made by the Bayesian brain (Cao et al., 2019); because the brain does not consider HL as salient, it does not update missing auditory information via the retrieval of parahippocampal memories.

The difference in tinnitus generation between the HL-T and HL-NT groups may be explained as follows: (a) when the brain detects decreased auditory input and the prefrontal "Bayesian inferential system" is active enough to fill in for the decreased peripheral sensory input to reduce uncertainty, and regards it as a sufficiently salient event, to generate phantom auditory perception by retrieving auditory memories stored in the parahippocampus, the brain ultimately generates tinnitus (the HL-T group); whereas (b) when the DMN of the brain surpasses the Bayesian inferential system and thus auditory memory retrieval is interrupted, the subject does not perceive tinnitus (the HL-NT group).

Using a volume entropy model of the brain, the present study uncovered different patterns of cortical information flow that may regulate tinnitus perception in individuals with HL. The increased information flow seen in the prefrontal Bayesian inferential network in the HL-T group suggests that HL was treated as an event of sufficient salience to generate phantom auditory perception, by retrieving auditory memories from the parahippocampus; thus, tinnitus is perceived. In contrast, in the HL-NT subjects, activation of the DMN prevented Bayesian inference and thus the generation of phantom auditory perception. In other words, the present study suggests that the balance of activity between the Bayesian inferential network and DMN determines whether tinnitus is generated in a brain with decreased peripheral auditory input. Follow-up neuromodulatory studies of the cortical areas responsible for tinnitus generation, and investigation of changes in volume entropy in the brain, could validate the current findings.

The current study has several limitations that should be addressed in future follow-up studies. First, 44 out of 65 subjects had

bilateral tinnitus while the other 21 had unilateral tinnitus. Because the laterality of tinnitus may have affected the results (Vanneste, Plazier, van der Loo, Van de Heyning, & De Ridder, 2011), follow-up studies in tinnitus subjects with homogenous laterality should be performed. Second, the male to female ratio of the two study groups showed statistically significant difference. This may have biased the results of the current study since male- and female tinnitus patients show different cortical, prefrontal, in particular, activity patterns (Vanneste, Joos, & De Ridder, 2012). Future studies controlled for the sex ratio should be performed to check the reproducibility of the current study. Third, future studies subdividing the HL-T group into low- and high-distressed tinnitus or acute- or chronic tinnitus may give us further information on other culprit brain areas of tinnitus generation such as the posterior cingulate cortex (PCC), based on previous qEEG studies showing connectivity changes in the PCC according to the chronicity of tinnitus (Lan et al., 2021) or the level of tinnitus-related distress (Vanneste & De Ridder, 2015b).

5 | CONCLUSION

Taken together, the current study suggests that the balance of activity between the Bayesian inferential network (updating missing auditory information by retrieving auditory memories from the hippocampus/parahippocampus) and DMN (maintaining the "silent status quo") determines whether phantom auditory perception occurs in a brain with decreased peripheral auditory input using the volume entropy model of the brain. Also, this study could be applied for treating tinnitus by offering potential target areas for neuromodulatory approaches.

ACKNOWLEDGMENTS

This work was supported by grants from the National Research Foundation of Korea (NRF) grant funded by the Korea government (MSIT) (grant number 2019R1A2C2004941, 2017R1E1A1A03070779), Seoul National University Bundang Hospital (14-2019-033), Industrial and Mathematical Data Analytics Research Center (IMDARC) (0679-20200002), and BK21 PLUS SNU Mathematical Sciences Division.

DISCLOSURE OF INTERESTS

The authors declare that we have no competing interests.

DATA AVAILABILITY STATEMENT

The data that support the findings of this study are available from the corresponding author upon reasonable request.

ORCID

Jae-Jin Song https://orcid.org/0000-0002-6631-3232
Sven Vanneste https://orcid.org/0000-0003-1513-5752

REFERENCES

Axelsson, A., & Ringdahl, A. (1989). Tinnitus–a study of its prevalence and characteristics. *British Journal of Audiology*, *23*, 53–62.

Baguley, D., McFerran, D., & Hall, D. (2013). Tinnitus. *Lancet*, *382*, 1600–1607.

Barry, R. J., Clarke, A. R., & Johnstone, S. J. (2011). Caffeine and opening the eyes have additive effects on resting arousal measures. *Clinical Neurophysiology*, *122*, 2010–2015.

Beissner, F., Meissner, K., Bar, K. J., & Napadow, V. (2013). The autonomic brain: An activation likelihood estimation meta-analysis for central processing of autonomic function. *The Journal of Neuroscience*, *33*, 10503–10511.

Boorman, E. D., Behrens, T. E., Woolrich, M. W., & Rushworth, M. F. (2009). How green is the grass on the other side? Frontopolar cortex and the evidence in favor of alternative courses of action. *Neuron*, *62*, 733–743.

Bossaerts, P. (2010). Risk and risk prediction error signals in anterior insula. *Brain Structure & Function*, *214*, 645–653.

Boutros, N. N., Mears, R., Pflieger, M. E., Moxon, K. A., Ludowig, E., & Rosburg, T. (2008). Sensory gating in the human hippocampal and rhinal regions: Regional differences. *Hippocampus*, *18*, 310–316.

Cao, Y., Summerfield, C., Park, H., Giordano, B. L., & Kayser, C. (2019). Causal inference in the multisensory brain. *Neuron*, *102*, 1076, e1078–1087.

Christopoulos, G. I., Tobler, P. N., Bossaerts, P., Dolan, R. J., & Schultz, W. (2009). Neural correlates of value, risk, and risk aversion contributing to decision making under risk. *The Journal of Neuroscience*, *29*, 12574–12583.

Clithero, J. A., & Rangel, A. (2014). Informatic parcellation of the network involved in the computation of subjective value. *Social Cognitive and Affective Neuroscience*, *9*, 1289–1302.

De Ridder, D., Elgoyhen, A. B., Romo, R., & Langguth, B. (2011). Phantom percepts: Tinnitus and pain as persisting aversive memory networks. *Proceedings of the National Academy of Sciences of the United States of America*, *108*, 8075–8080.

De Ridder, D., Fransen, H., Francois, O., Sunaert, S., Kovacs, S., & Van De Heyning, P. (2006). Amygdalohippocampal involvement in tinnitus and auditory memory. *Acta Oto-Laryngologica. Supplementum*, *126*, 50–53.

De Ridder, D., Joos, K., & Vanneste, S. (2014). The enigma of the tinnitus-free dream state in a Bayesian world. *Neural Plasticity*, *2014*, 612147.

De Ridder, D., Vanneste, S., & Freeman, W. (2014). The Bayesian brain: Phantom percepts resolve sensory uncertainty. *Neuroscience and Biobehavioral Reviews*, *44*, 4–15.

Donoso, M., Collins, A. G., & Koechlin, E. (2014). Human cognition. Foundations of human reasoning in the prefrontal cortex. *Science*, *344*, 1481–1486.

Eggermont, J. J., & Kral, A. (2016). Somatic memory and gain increase as preconditions for tinnitus: Insights from congenital deafness. *Hearing Research*, *333*, 37–48.

Eggermont, J. J., & Roberts, L. E. (2012). The neuroscience of tinnitus: Understanding abnormal and normal auditory perception. *Frontiers in Systems Neuroscience*, *6*, 53.

Fox, J. M., Abram, S. V., Reilly, J. L., Eack, S., Goldman, M. B., Csernansky, J. G., … Smith, M. J. (2017). Default mode functional connectivity is associated with social functioning in schizophrenia. *Journal of Abnormal Psychology*, *126*, 392–405.

Foxe, J. J., Morie, K. P., Laud, P. J., Rowson, M. J., de Bruin, E. A., & Kelly, S. P. (2012). Assessing the effects of caffeine and theanine on the maintenance of vigilance during a sustained attention task. *Neuropharmacology*, *62*, 2320–2327.

Friston, K. (2010). The free-energy principle: A unified brain theory? *Nature Reviews. Neuroscience*, *11*, 127–138.

Gallus, S., Lugo, A., Garavello, W., Bosetti, C., Santoro, E., Colombo, P., … Langguth, B. (2015). Prevalence and determinants of tinnitus in the Italian adult population. *Neuroepidemiology*, *45*, 12–19.

Han, J. J., Jang, J. H., Ridder, D., Vanneste, S., Koo, J. W., & Song, J. J. (2018). Increased parietal circuit-breaker activity in delta frequency band and abnormal delta/theta band connectivity in salience network in hyperacusis subjects. *PLoS One*, *13*, e0191858.

Han, J. J., Ridder, D., Vanneste, S., Chen, Y. C., Koo, J. W., & Song, J. J. (2020). Pre-treatment ongoing cortical oscillatory activity predicts improvement of tinnitus after partial peripheral Reafferentation with hearing aids. *Frontiers in Neuroscience*, *14*, 410.

Hullfish, J., Sedley, W., & Vanneste, S. (2019). Prediction and perception: Insights for (and from) tinnitus. *Neuroscience and Biobehavioral Reviews*, *102*, 1–12.

Joos, K., Vanneste, S., & De Ridder, D. (2012). Disentangling depression and distress networks in the tinnitus brain. *PLoS One*, *7*, e40544.

Kim, H. J., Lee, H. J., An, S. Y., Sim, S., Park, B., Kim, S. W., … Choi, H. G. (2015). Analysis of the prevalence and associated risk factors of tinnitus in adults. *PLoS One*, *10*, e0127578.

Kim, S. H., Jang, J. H., Lee, S. Y., Han, J. J., Koo, J. W., Vanneste, S., … Song, J. J. (2016). Neural substrates predicting short-term improvement of tinnitus loudness and distress after modified tinnitus retraining therapy. *Scientific Reports*, *6*, 29140.

Lan, L., Li, J., Chen, Y., Chen, W., Li, W., Zhao, F., … others. (2021). Alterations of brain activity and functional connectivity in transition from acute to chronic tinnitus. *Human Brain Mapping*, *42*, 485–494.

Lee, H., Kim, E., Ha, S., Kang, H., Huh, Y., Lee, Y., … Lee, D. S. (2019). Volume entropy for modeling information flow in a brain graph. *Scientific Reports*, *9*, 256.

Lee, S. Y., Choi, B. Y., Koo, J. W., De Ridder, D., & Song, J. J. (2020). Cortical oscillatory signatures reveal the prerequisites for tinnitus perception: A comparison of subjects with sudden Sensorineural hearing loss with and without tinnitus. *Frontiers in Neuroscience*, *14*, 596647.

Lee, S. Y., Nam, D. W., Koo, J. W., De Ridder, D., Vanneste, S., & Song, J. J. (2017). No auditory experience, no tinnitus: Lessons from subjects with congenital- and acquired single-sided deafness. *Hearing Research*, *354*, 9–15.

Lee, S. Y., Rhee, J., Shim, Y. J., Kim, Y., Koo, J. W., De Ridder, D., … Song, J. J. (2019). Changes in the resting-state cortical oscillatory activity 6 months after modified tinnitus retraining therapy. *Frontiers in Neuroscience*, *13*, 1123.

Lim, S. (2008). Minimal volume entropy for graphs. *Transactions of the American Mathematical Society*, *360*, 5089–5100.

Moazami-Goudarzi, M., Michels, L., Weisz, N., & Jeanmonod, D. (2010). Temporo-insular enhancement of EEG low and high frequencies in patients with chronic tinnitus. QEEG study of chronic tinnitus patients. *BMC Neuroscience*, *11*, 40.

Mohan, A., De Ridder, D., & Vanneste, S. (2016). Emerging hubs in phantom perception connectomics. *Neuroimage Clinic*, *11*, 181–194.

Moulton, E. A., Elman, I., Pendse, G., Schmahmann, J., Becerra, L., & Borsook, D. (2011). Aversion-related circuitry in the cerebellum: Responses to noxious heat and unpleasant images. *The Journal of Neuroscience*, *31*, 3795–3804.

Murphy, C., Jefferies, E., Rueschemeyer, S. A., Sormaz, M., Wang, H. T., Margulies, D. S., & Smallwood, J. (2018). Distant from input: Evidence of regions within the default mode network supporting perceptually-decoupled and conceptually-guided cognition. *NeuroImage*, *171*, 393–401.

Newman, M. E. J, Strogatz, S. H., & Watts, D. J. (2001). Random graphs with arbitrary degree distributions and their applications. *Physical Review E*, *64*(2). https://doi.org/10.1103/PhysRevE.64.026118.

Norena, A., Micheyl, C., Chery-Croze, S., & Collet, L. (2002). Psychoacoustic characterization of the tinnitus spectrum: Implications for the underlying mechanisms of tinnitus. *Audiology & Neuro-Otology*, *7*, 358–369.

Norena, A. J., & Eggermont, J. J. (2005). Enriched acoustic environment after noise trauma reduces hearing loss and prevents cortical map reorganization. *The Journal of Neuroscience*, *25*, 699–705.

Oiticica, J., & Bittar, R. S. (2015). Tinnitus prevalence in the city of Sao Paulo. *Brazilian Journal of Otorhinolaryngology*, *81*, 167–176.

Pearson, J. M., Heilbronner, S. R., Barack, D. L., Hayden, B. Y., & Platt, M. L. (2011). Posterior cingulate cortex: Adapting behavior to a changing world. *Trends in Cognitive Sciences*, *15*, 143–151.

Raichle, M. E., MacLeod, A. M., Snyder, A. Z., Powers, W. J., Gusnard, D. A., & Shulman, G. L. (2001). A default mode of brain function. *Proceedings of the National Academy of Sciences of the United States of America*, *98*, 676–682.

Raichle, M. E., & Snyder, A. Z. (2007). A default mode of brain function: A brief history of an evolving idea. *NeuroImage*, *37*, 1083–1090 discussion 1097-1089.

Schaette, R., Turtle, C., & Munro, K. J. (2012). Reversible induction of phantom auditory sensations through simulated unilateral hearing loss. *PLoS One*, *7*, e35238.

Schecklmann, M., Vielsmeier, V., Steffens, T., Landgrebe, M., Langguth, B., & Kleinjung, T. (2012). Relationship between audiometric slope and tinnitus pitch in tinnitus patients: Insights into the mechanisms of tinnitus generation. *PLoS One*, *7*, e34878.

Seeley, W. W., Menon, V., Schatzberg, A. F., Keller, J., Glover, G. H., Kenna, H., … Greicius, M. D. (2007). Dissociable intrinsic connectivity networks for salience processing and executive control. *The Journal of Neuroscience*, *27*, 2349–2356.

Shargorodsky, J., Curhan, G. C., & Farwell, W. R. (2010). Prevalence and characteristics of tinnitus among US adults. *The American Journal of Medicine*, *123*, 711–718.

Sherlin, L., & Congedo, M. (2005). Obsessive-compulsive dimension localized using low-resolution brain electromagnetic tomography (LORETA). *Neuroscience Letters*, *387*, 72–74.

Shulman, G. L., Fiez, J. A., Corbetta, M., Buckner, R. L., Miezin, F. M., Raichle, M. E., & Petersen, S. E. (1997). Common blood flow changes across visual tasks: II. Decreases in cerebral cortex. *Journal of Cognitive Neuroscience*, *9*, 648–663.

Song, J. J., Kim, K., Sunwoo, W., Mertens, G., Van de Heyning, P., De Ridder, D., et al. (2017). A quantitative electroencephalography study on Cochlear implant-induced cortical changes in single-sided deafness with tinnitus. *Frontiers in Human Neuroscience*, *11*, 210.

Tolman, E. C. (1948). Cognitive maps in rats and men. *Psychological Review*, *55*, 189–208.

Tulving, E., & Markowitsch, H. J. (1997). Memory beyond the hippocampus. *Current Opinion in Neurobiology*, *7*, 209–216.

Vanneste, S., Alsalman, O., & De Ridder, D. (2019). Top-down and bottom-up regulated auditory phantom perception. *The Journal of Neuroscience*, *39*, 364–378.

Vanneste, S., & De Ridder, D. (2012). The use of alcohol as a moderator for tinnitus-related distress. *Brain Topography*, *25*, 97–105.

Vanneste, S., & De Ridder, D. (2015a). Stress-related functional connectivity changes between auditory cortex and cingulate in tinnitus. *Brain Connectivity*, *5*, 371–383.

Vanneste, S., & De Ridder, D. (2016). Deafferentation-based pathophysiological differences in phantom sound: Tinnitus with and without hearing loss. *NeuroImage*, *129*, 80–94.

Vanneste, S., Joos, K., & De Ridder, D. (2012). Prefrontal cortex based sex differences in tinnitus perception: Same tinnitus intensity, same tinnitus distress, different mood. *PLoS One*, *7*, e31182.

Vanneste, S., Plazier, M., van der Loo, E., Van de Heyning, P., & De Ridder, D. (2011). The difference between uni- and bilateral auditory phantom percept. *Clinical Neurophysiology*, *122*, 578–587.

Vanneste, S., Song, J. J., & De Ridder, D. (2018). Thalamocortical dysrhythmia detected by machine learning. *Nature Communications*, *9*, 1103.

Vanneste, S., To WT, & De Ridder, D. (2019). Tinnitus and neuropathic pain share a common neural substrate in the form of specific brain connectivity and microstate profiles. *Progress in Neuro-Psychopharmacology & Biological Psychiatry*, *88*, 388–400.

Wang, R. W. Y., Chang, W. L., Chuang, S. W., & Liu, I. N. (2019). Posterior cingulate cortex can be a regulatory modulator of the default mode network in task-negative state. *Scientific Reports*, *9*, 7565.

Wasserman, L. (2013). *All of statistics: A concise course in statistical inference*. New York, NY: Springer Science & Business Media.

Weilnhammer, V. A., Stuke, H., Sterzer, P., & Schmack, K. (2018). The neural correlates of hierarchical predictions for perceptual decisions. *The Journal of Neuroscience*, *38*, 5008–5021.

Wikenheiser, A. M., & Schoenbaum, G. (2016). Over the river, through the woods: Cognitive maps in the hippocampus and orbitofrontal cortex. *Nature Reviews. Neuroscience*, *17*, 513–523.

Wu, B. P., Searchfield, G., Exeter, D. J., & Lee, A. (2015). Tinnitus prevalence in New Zealand. *The New Zealand Medical Journal*, *128*, 24–34.

Xu, X., Yuan, H., & Lei, X. (2016). Activation and connectivity within the default mode network contribute independently to future-oriented thought. *Scientific Reports*, *6*, 21001.

How to cite this article: Song, J.-J., Park, J., Koo, J.-W., Lee, S.-Y., Vanneste, S., De Ridder, D., Hong, S., & Lim, S. (2021). The balance between Bayesian inference and default mode determines the generation of tinnitus from decreased auditory input: A volume entropy-based study. *Human Brain Mapping*, 1–15. https://doi.org/10.1002/hbm.25539